PAPER

Single crystal growth of $Mn_4Nb_2O_9$ and its structure-magnetic coupling

Yiming Cao,[abc] Maolin Xiang,[b] Zhenjie Feng,[b] Baojuan Kang,[b] Jincang Zhang,[de] Nicolas Guiblin,[c] Wei Ren,[bde] Brahim Dkhil*[c] and Shixun Cao*[bde]

A single crystal of $Mn_4Nb_2O_9$ of about 8 mm in diameter and 30 mm in length was successfully grown by a newly designed one-step method based on the optical floating zone technique. Clear Laue spots and sharp XRD Bragg reflections attest the good crystal quality. The antiferromagnetic phase transition at T_N = 108.4 K of the $Mn_4Nb_2O_9$ single crystal was observed along the c axis, which contrasts with $Co_4Nb_2O_9$ belonging to the same structural family. Structural changes with a-axis shrinkage and c-axis expansion at T_N demonstrate a significant and anisotropic magnetostriction effect.

Introduction

Recently, $A_4B_2O_9$ (A = Co, Mn, B = Nb, Ta) have attracted more attention due to their spin flop phase transition,[1] magneto-dielectric effect[1] and magnetoelectric effect.[2] $Mn_4Nb_2O_9$ was first prepared and studied by Bertaut *et al.*[3] X-ray diffraction (XRD) studies showed that $Mn_4Nb_2O_9$ possesses a trigonal crystal structure (space group $P\bar{3}c1$) with two formula units per cell. The magnetic structure of $Mn_4Nb_2O_9$ has also been reported by Bertaut *et al.*[3] and further confirmed by Schwarz *et al.*[4] According to the results of neutron diffraction, below Néel temperature (about 125 K), Mn spins order along the c axis and form chains along the lines $\frac{1}{3}\frac{2}{3}z$ (+spins) and $\frac{2}{3}\frac{1}{3}z$ (−spins) with antiparallel inter-chain coupling.

The study and confirmation of the magnetoelectric effect in these compounds were conducted by Fischer *et al.*[5] Furthermore, magneto-dielectric effect and magnetic-induced electric polarization were observed in polycrystalline $Mn_4Nb_2O_9$ by Fang *et al.*[6] However, detailed data about the physical properties of the single crystal $Mn_4Nb_2O_9$ are still lacking to further understand this material. In this work, we grow successfully single crystal of $Mn_4Nb_2O_9$ samples by our newly designed one-step method based on the optical floating zone technique. A single crystal with well-defined crystallographic orientation allows us

to investigate the anisotropy of its magnetic and structural properties. The crystallographic orientations were identified by both Laue X-ray photography and X-ray diffraction. An antiferromagnetic (AFM) transition is found at Néel temperature T_N = 108.4 K. In contrast to $Co_4Nb_2O_9$,[7] the AFM order of $Mn_4Nb_2O_9$ single crystal is along c axis and the spin flop transition does not occur even with a magnetic field up to 7 T. A structural phase transition is observed with a-direction shrinkage and c-direction expansion around 110 K, which corresponds exactly to the T_N of $Mn_4Nb_2O_9$. The magnetic structure of our AFM $Co_4Nb_2O_9$ single crystal is different from a collinear arrangement with spin parallel to the trigonal axis as proposed previously by Bertaut *et al.*[3] and resembles the Co^{2+} magnetic moments found to be almost lying in the basal plane by Khanh *et al.*[8] But the main difference between the samples, which is responsible for the different easy axis directions, is not clear yet.

Experimental details

Polycrystalline $Mn_4Nb_2O_9$ decomposes easily, so that it is difficult to synthesize by conventional solid-state reaction technique. Here, a one-step method based on the optical floating zone technique was designed to grow the single crystal of $Mn_4Nb_2O_9$. The stoichiometric mixtures of Nb_2O_5 (99.99% @ Alfa Aesar) and $MnCO_3$ (99.9% @ Alfa Aesar) powders were well grounded and calcined at a temperature of 900 °C for 6 h under the protection of Ar gas flow. The milled pre-sintered material (that is a mixture of $MnNb_2O_6$ and Mn_3O_4 confirmed by XRD) was isostatically pressed into a cylindrical shape of 70 mm length and 8 mm diameter at 70 MPa and sintered at 1100 °C at a rate of 2 °C min^{-1} for 12 h. Single crystal of $Mn_4Nb_2O_9$ was then successfully grown in an optical floating zone furnace (FZ-T-10000-H-VI-P-SH, Crystal Systems Corp.) with 4 × 1000 W halogen lamps installed as infrared radiation sources by using the rod of the above prepared mixture. The temperature of the molten zone focused by mirrors was

[a]Center for Magnetic Materials and Devices and Key Laboratory for Advanced Functional and Low Dimensional Materials of Yunnan Higher Education Institute, Qujing Normal University, 655011, China

[b]Department of Physics, International Center of Quantum and Molecular Structures, Shanghai University, Shanghai 200444, China. E-mail: sxcao@shu.edu.cn

[c]Laboratoire Structures, Propriétés et Modélisation des Solides, CentraleSupélec, CNRS-UMR 8580, Université Paris-Saclay, 92295 Châtenay-Malabry Cedex, France. E-mail: brahim.dkhil@centralesupelec.fr

[d]Materials Genome Institute, Shanghai University, Shanghai 200444, China

[e]Shanghai Key Laboratory of High Temperature Superconductors, Shanghai University, Shanghai 200444, China
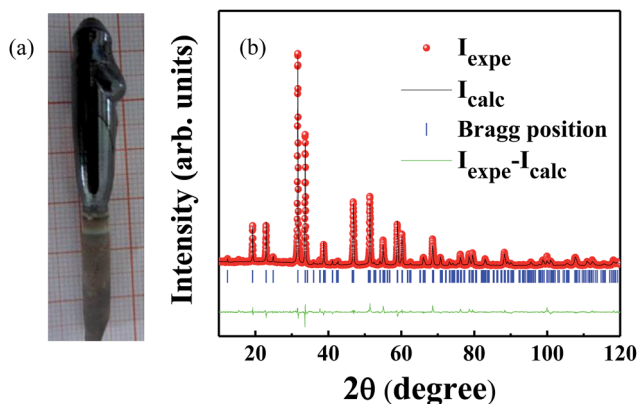
Fig. 1 (a) Picture of the as-grown single crystal of $Mn_4Nb_2O_9$; (b) powder X-ray diffractogram from ground single crystal $Mn_4Nb_2O_9$ showing the experimental, calculated, and difference intensities along with the Bragg positions.

precisely controlled by adjusting the power of the lamps. During the growth, the molten zone was moved upwards at a rate of 5 mm h^{-1}, with the seed rod (lower shaft) and the feed rod (upper shaft) counter rotating at 30 rpm in Ar gas flow by 4 L min^{-1}. A single crystal of $Mn_4Nb_2O_9$ of about 8 mm in diameter and 30 mm in length with black shining surface was obtained, as shown in Fig. 1a. The room temperature crystal structure was characterized by XRD (XRD, D/max2200) using Cu Kα radiation. Low temperature XRD data were collected with a high accuracy home-made Bragg–Brentano diffractometer equipped with a copper source monochromatic radiation $\lambda = 1.54056$ Å issued from a 18 kW Rigaku rotating anode, from 90 K to 900 K under air atmosphere by using a cryofurnace and a furnace with an accuracy better than 0.1 K and 2 K, respectively. Variation of temperature steps is 5 K from 90 K to 150 K. The step is 0.02° and integration time is 4 s, respectively. Crystallographic orientation was determined by using back-reflection Laue X-ray photography with tungsten target (with the X-ray beam of 0.5 mm in diameter) and additionally confirmed by standard XRD. Measurements of the magnetization were conducted using a Physical Property Measurement System (PPMS-9, Quantum Design Inc.) with Vibrating Sample Magnetometer (VSM) option. The temperature and magnetic field increasing/decreasing rates are 1.5 K min^{-1} and 0.01 T s^{-1}, respectively. The temperature and magnetic field ranges are 2–400 K and −9 to 9 T, respectively. The sensitivity of the VSM is 10^{-9} A m^2.

Results and discussion

Rietveld method[9] as implemented in the FullProf program[10] was used for the refinement of the structure parameters, based on the powder (ground single crystal by agate mortar) XRD data of $Mn_4Nb_2O_9$ as shown in Fig. 1b. The powder diffraction patterns can be assigned to a single-phase corundum trigonal crystal structure[11] with $P\bar{3}c1$ space group which is similar to that of $Co_4Nb_2O_9$.[2,7,8] The lattice parameters obtained are $a = b = 5.32449 \pm 0.00016$ Å and $c = 14.32222 \pm 0.00043$ Å. The unit cell of $Mn_4Nb_2O_9$ is thus larger than that of $Co_4Nb_2O_9$ and this is due to the slightly larger ionic radius of Mn^{2+} with respect to that of Co^{2+}.

Fig. 2a and b show the XRD patterns with θ–2θ scans recorded on slices cut perpendicular to the a and c axes which have been identified by using back-reflection Laue photograph (see inset of Fig. 2a and b). As it is shown in Fig. 2a and b, four $(h00)$ $(h = 1, 2, 3, 4)$ and six $(00l)$ $(l = 2, 4, 6, 8, 10, 12)$ reflections, respectively can be easily indexed. The sharp XRD peaks with no impurity or misorientation detected as well as the clear Laue diffraction spots imply high quality $Mn_4Nb_2O_9$ single crystal.

In order to check the magnetic properties of $Mn_4Nb_2O_9$, and because $Mn_4Nb_2O_9$ displays nonequivalence between a axis and c axis, similarly to $Co_4Nb_2O_9$, temperature dependence of $M_a(T)$ and $M_c(T)$ was measured under a small magnetic field $H = 0.01$ T applied along a and c axes of $Mn_4Nb_2O_9$ single crystal as shown in Fig. 3a. $Mn_4Nb_2O_9$ shows a strong magnetic anisotropy which leads to dramatically different temperature dependence of $M_a(T)$ and $M_c(T)$. With the decrease of the temperature, $M_c(T)$ exhibits a magnetic Néel transition around $T_N = 108.4$ K, which corresponds to the previously observed AFM transition in polycrystalline $Mn_4Nb_2O_9$, but for which the orientation of the magnetic moments[6] could not be identified. Below T_N, $M_c(T)$ decreases linearly with temperature down to 3 K. On the contrary, $M_a(T)$ presents the same increasing trend upon cooling of temperature even below T_N. This suggests that the antiferromagnetic axis of $Mn_4Nb_2O_9$ is not same as that of $Co_4Nb_2O_9$ along a axis and therefore, the magnetic structure of both compounds must be different. The magnetic structure of
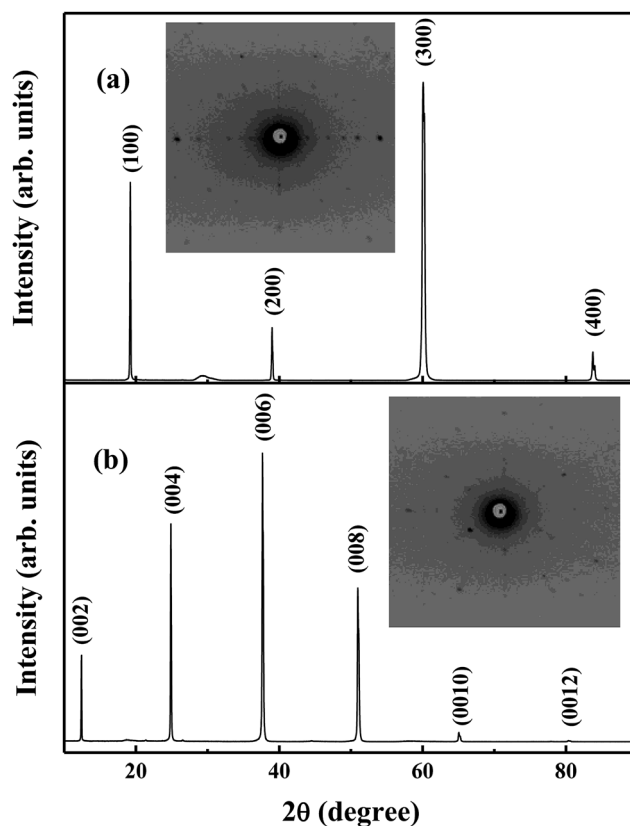

Fig. 2 XRD patterns of single crystal $Mn_4Nb_2O_9$ along the a (a) and c (b) axis. The insets show corresponding Laue photographs of the a and c axis.
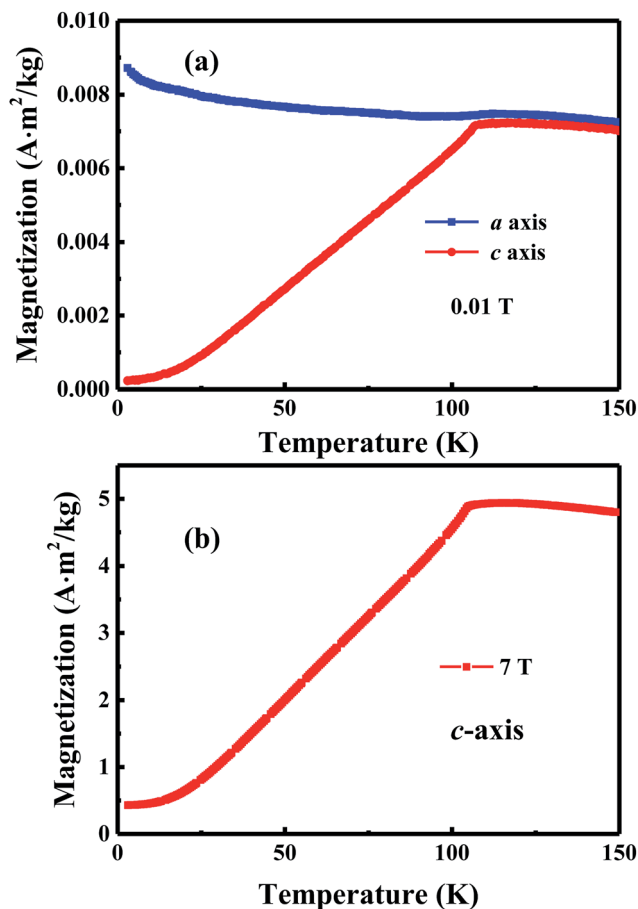
Fig. 3 Temperature dependence of the magnetization $M(T)$ of $Mn_4Nb_2O_9$ measured along a and c axis under an applied magnetic field of 0.01 T (a) and along c axis under a magnetic field of 7 T (b).

Fig. 4 Magnetic field dependence of the magnetization $M(H)$ of $Mn_4Nb_2O_9$ measured along a (a) and c (b) axis at 5 K.

$Mn_4Nb_2O_9$ given by Bertaut et $al.$[3] where Mn spins align to the c axis and form chains along the lines $\frac{1}{3}\frac{2}{3}z$ (+spins) and $\frac{2}{3}\frac{1}{3}z$ (−spins) with antiparallel inter-chain coupling can be thus used to explain the magnetic measurements of $Mn_4Nb_2O_9$.

To reveal the occurrence of the spin flop in $Mn_4Nb_2O_9$ single crystal, we further measured magnetization curves under a strong external field ($H = 7$ T) along c axis. As shown in Fig. 3b, the behavior is different from $Co_4Nb_2O_9$ as $M_c(T)$ here shows no change with comparison to $M_c(T)$ measurement under a field of $H = 0.01$ T. This demonstrates that the spin flop does not occur along c axis even though the applied magnetic field is up to 7 T.

Furthermore, the magnetic field dependences of the magnetization along a and c axes at 5 K were measured (Fig. 4). A linear $M_a(H)$ curve with no slope abnormality is shown in Fig. 4a indicating that there is no antiferromagnetic ordering component along the a axis. In Fig. 4b, although there is a deviation from the linear behavior in $M_c(H)$ curve at around 4 T, the induced magnetization is not reached up to 7 T which confirms that the critical magnetic field to induce the spin flop transition in single crystal $Mn_4Nb_2O_9$ is larger than 7 T. There is no doubt that the critical magnetic field of single crystal $Mn_4Nb_2O_9$ is much larger than 0.75 T found in single crystal
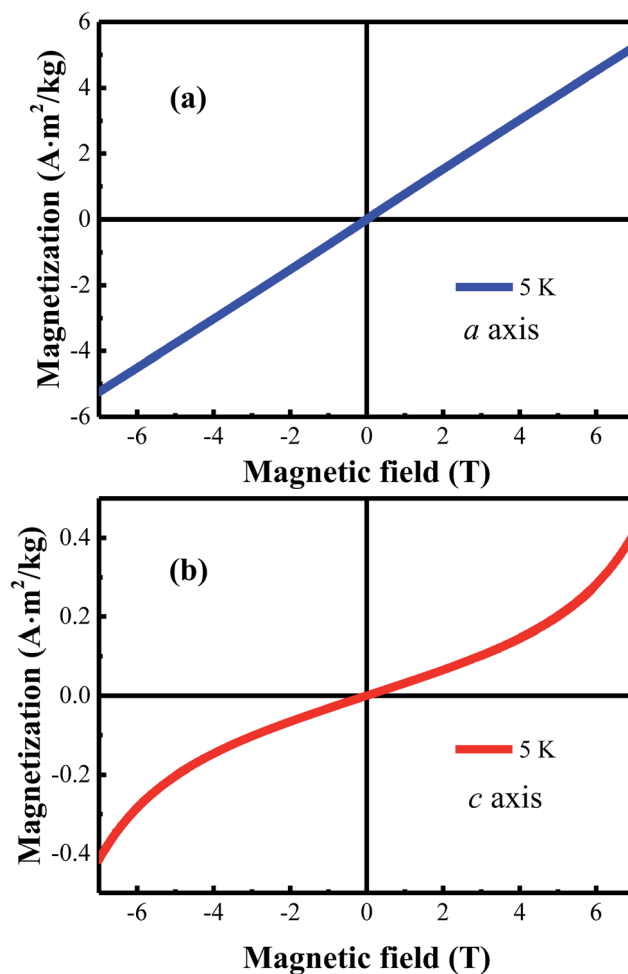
$Co_4Nb_2O_9$. The Zeeman energy which induces the spin flop can be expressed as:[12]

$$E_{Zeeman} = -\mu_0 M_{Net} H_{Ext} \cos \theta \qquad (1)$$

where μ_0, M_{Net}, H_{Ext}, and θ represent respectively the vacuum permeability, the magnetic moments of Mn^{2+}, the external magnetic field, and the angle between M_{Net} and H_{Ext}. The magnetic moment of Mn^{2+} is known to be larger than that of Co^{2+}.[13] The θ angle for both $Co_4Nb_2O_9$ and $Mn_4Nb_2O_9$ is π as the magnetic moments of Co^{2+} and Mn^{2+} in $Co_4Nb_2O_9$ and $Mn_4Nb_2O_9$ align in antiferromagnetic configurations along a and c axis, respectively. The Zeeman energy of $Mn_4Nb_2O_9$ is thus larger than that of $Co_4Nb_2O_9$ under the same external magnetic field. The antiferromagnetic coupling between the magnetic moments of Mn^{2+} is larger than the difference of Zeeman energy between both systems. Therefore, $Mn_4Nb_2O_9$ requires a larger critical magnetic field to induce the spin flop metamagnetic transition.

In order to check if the antiferromagnetic phase transition is accompanied with structural changes, the (300) and (006) Bragg reflections along a and c axis, respectively were measured by
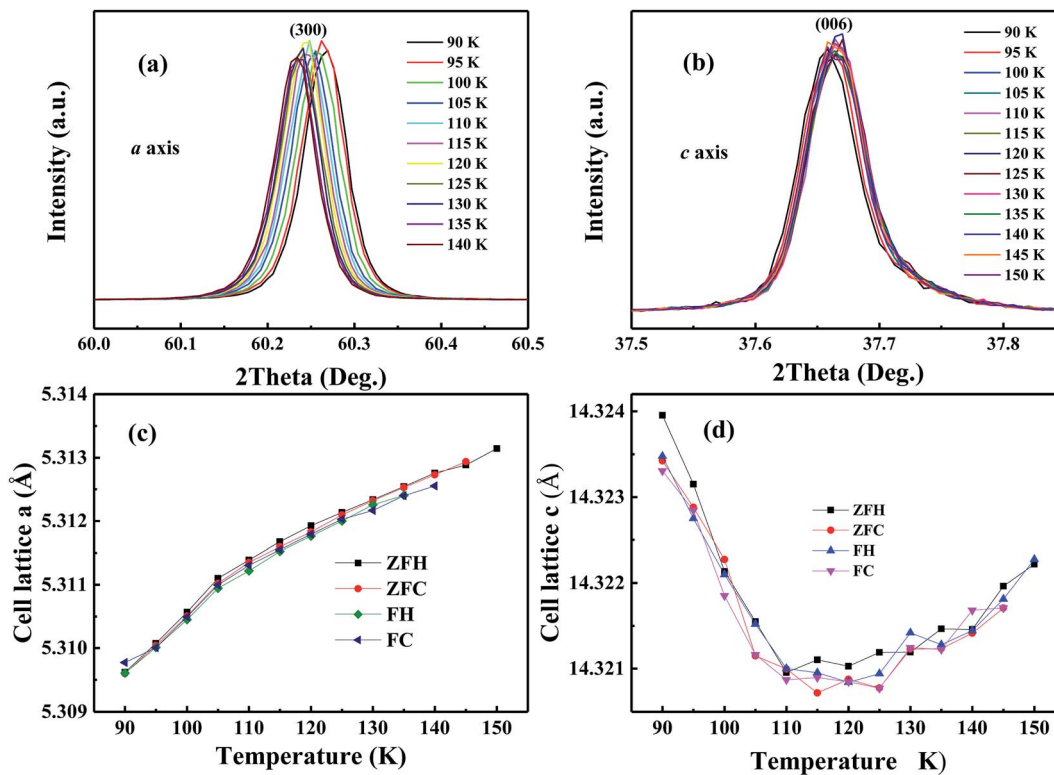
Fig. 5 XRD data of (300) and (006) Bragg reflections as a function of temperature along *a* (a) and *c* (b) axis, respectively. (c) and (d) show corresponding *a* and *c* lattice parameters as a function of temperature. ZFC/ZFH, FC and FH indicate the zero electric field cooling/heating, electric field cooling and field heating regimes, respectively. The electric field value used is 20 kV cm^{-1}.

varying the temperature. As shown in Fig. 5a, the (300) Bragg reflections shift towards higher 2θ degrees by decreasing the temperature. In contrast to (300) Bragg reflections, the (006) Bragg reflections first shift to higher 2θ angles on cooling and then shift to lower 2θ degrees as shown in Fig. 5b. The peak positions of the Bragg reflections can then be obtained by fitting the corresponding (300) and (006) Bragg reflections using Gaussian function fitting. The *a* and *c* lattice parameters as a function of temperature between 90 K and 150 K are plotted in Fig. 5c and d, respectively. As the temperature decreases, there is a structural change of a shrinkage along *a* direction while an expansion along *c* direction below around 110 K which is exactly the T_N of $Mn_4Nb_2O_9$ evidenced above using magnetic measurements. There is therefore an obvious magnetostriction effect occurring at the AFM phase transition. This result is appealing to further investigations for instance by studying the magnetic behavior under pressure/stress and/ or the resulting strain under magnetic field. Furthermore, if the structure-magnetic coupling is strong enough, it opens the door towards strain-engineering of the magnetism in $Mn_4Nb_2O_9$. Finally, we also applied an electric field of 20 kV cm^{-1}, within field cooling (FC) and field heating (FH) regimes and followed the Bragg reflections *versus* temperature (Fig. 5c and d). However, there is no distinction between the data under electric field (FC, FH) and those without or zero (ZFC and ZFH) field regime, indicating that no magnetoelectric coupling exists in $Mn_4Nb_2O_9$.

Conclusion

In summary, we have successfully synthesized $Mn_4Nb_2O_9$ single crystal with a single phase of corundum-type structure by a one-step method based on the optical floating zone technique. Characterizations of the crystal by X-ray diffraction and Laue photographs analysis show the good quality of the crystal. An antiferromagnetic phase transition is found at Néel temperature $T_N = 108.4$ K. In contrast to $Co_4Nb_2O_9$, such AFM ordering is along *c* axis and the spin flop transition cannot be achieved with magnetic field up to 7 T. A structural modification with shrinking of the *a* direction and expansion of *c* direction takes place at T_N and indicates a magnetostriction effect. We also applied an electric field across the magnetic transition showing that no magnetoelectric coupling exists. Further work is needed to study the interaction between structure and magnetism in $Mn_4Nb_2O_9$ single crystal.

Acknowledgements

References

1 T. Kolodiazhnyi, H. Sakurai and N. Vittayakorn, *Appl. Phys. Lett.*, 2011, **99**, 132906.

2 Y. Fang, Y. Q. Song, W. P. Zhou, R. Zhao, R. J. Tang, H. Yang, L. Y. Lv, S. G. Yang, D. H. Wang and Y. W. Du, *Sci. Rep.*, 2014, **4**, 3860.

3 E. F. Bertaut, L. Corliss, F. Forrat, R. Aleonard and R. Pauthenet, *J. Phys. Chem. Solids*, 1961, **21**, 234–251.

4 B. Schwarz, D. Kraft, R. Theissmann and H. Ehrenberg, *J. Magn. Magn. Mater.*, 2010, **322**, L1–L3.

5 E. Fischer, G. Gorodetsky and R. M. Hornreich, *Solid State Commun.*, 1972, **10**, 1127–1132.

6 Y. Fang, W. P. Zhou, S. M. Yan, R. Bai, Z. H. Qian, Q. Y. Xu, D. H. Wang and Y. W. Du, *J. Appl. Phys.*, 2015, **117**, 17b712.

7 Y. Cao, Y. Yang, M. Xiang, Z. Feng, B. Kang, J. Zhang, W. Ren and S. Cao, *J. Cryst. Growth*, 2015, **420**, 90–93.

8 N. D. Khanh, N. Abe, H. Sagayama, A. Nakao, T. Hanashima, R. Kiyanagi, Y. Tokunaga and T. Arima, *Phys. Rev. B*, 2016, **93**, 075117.

9 H. Rietveld, *Acta Crystallogr.*, 1967, **22**, 151–152.

10 J. Rodriguez-Carvajal, *Phys. B*, 1993, **192**, 55–69.

11 M. Ye and D. Vanderbilt, *Phys. Rev. B*, 2016, **93**, 134303.

12 Y. Cao, S. Cao, W. Ren, Z. Feng, S. Yuan, B. Kang, B. Lu and J. Zhang, *Appl. Phys. Lett.*, 2014, **104**, 232405.

13 K. Tomiyasu, J. Fukunaga and H. Suzuki, *Phys. Rev. B: Condens. Matter Mater. Phys.*, 2004, **70**, 214434.